SIMULATION-BASED DESIGN AND EVALUATION OF A DUAL-AXIS SOLAR-TRACKING MECHATRONIC SYSTEM FOR A 50-WATT-PEAK PANEL

Excellsdeo Jonathan Polii Ndahawali[1*], I Komang Ardika[2], Priyono[3], Tammy Tinny Veisy Pangow[4], Adriyan Warokka[5]
[12345] Politeknik Negeri Manado, Indonesia
*Corresponding Author: xclljonathan@gmail.com

ABSTRACT
Dual-axis photovoltaic tracking requires coordinated mechanical, electronic, control, and safety subsystems. This simulation-based design study develops an integrated mechatronic architecture for a 50 Wp panel using an Arduino Mega 2560, four light-dependent resistors, two 3 N·m closed-loop NEMA 23 motors, 20:1 worm reducers, 20T:60T timing pulleys, normally closed limit switches, an anemometer, an RTC DS3231, driver alarms, and a hardware emergency stop. The outer loop uses normalized azimuth and elevation light errors, an eight-sample moving-average filter, a deadband equivalent to 0.5°, and dominant-axis pulse scheduling; the inner motor loop uses encoder feedback, and a supervisory state machine manages INIT, HOMING, TRACKING, HOLD, PARK, STOW, and FAULT modes. A deterministic seven-day scenario was evaluated from 08:00 to 17:00, comprising ten hourly reporting points and nine one-hour integration intervals per day (70 reported observations). The environmental and orientation profiles were prescribed for design evaluation rather than sampled from a documented field site. Under these assumptions, the tracked-panel model produced 283.93 Wh/day versus 237.48 Wh/day for the fixed comparator, a descriptive gain of 19.56%. The model-residual combined RMSE was 0.158°, maximum residual error was 0.44°, estimated actuator consumption was 0.495 Wh/day, and estimated net gain was 45.95 Wh/day. These values describe internal model behavior, not validated hardware performance. No physical prototype, independent output-shaft measurement, stochastic uncertainty analysis, or location-specific economic assessment was conducted. The contribution is therefore a system-level integration and verification framework, together with explicit requirements for subsequent prototype and field validation.

Keywords: closed-loop control, deterministic simulation, dual-axis solar tracking, photovoltaic, supervisory state machine

INTRODUCTION

Photovoltaic modules convert solar radiation into electrical energy, but their output is affected by incidence angle, cell temperature, atmospheric conditions, electrical conversion losses, and load characteristics. A fixed panel reaches its most favorable orientation only during a limited part of the day. A dual-axis tracker can reduce this angular mismatch by adjusting azimuth and elevation, but an increase in gross panel energy is useful only when sensing, actuation, transmission, supervisory control, and protection operate as a coherent mechatronic system and when the energy required by tracking is explicitly accounted for.

Active solar-tracking methods are commonly grouped into open-loop solar-position methods, closed-loop light-sensor methods, and hybrid methods. International reviews emphasize that the choice among these approaches involves trade-offs in sensing uncertainty, algorithmic complexity, robustness to diffuse light and shading, calibration burden, and implementation cost (Awasthi et al., 2020; Fuentes-Morales et al., 2020). Four-LDR arrangements remain attractive for low-cost prototypes and laboratory applications, but raw readings are sensitive to irradiance level, local shadows, sensor mismatch, and electrical noise. Normalized errors, filtering, a deadband, and low-irradiance logic are therefore required to reduce threshold drift and actuator hunting (Jamroen et al., 2020). Broader reviews confirm that tracker selection should consider axis configuration, drive type, control strategy, sensing limitations, maintenance, and lifecycle cost (Al-Rousan et al., 2018; Hafez et al., 2018; Lee et al., 2009; Mousazadeh et al., 2009; Seme et al., 2020).

Indonesian studies show sustained interest in dual-axis photovoltaic trackers. Asmi and Candra (2020) used an Arduino Nano and four LDRs; Hakim and Sukma (2022) used an Arduino Mega

2560 and stepper motors; Dewanto et al. (2022) examined sensor number and tracking delay; Pardosi et al. (2024) reported an Arduino-based implementation; and Soedjangi (2025) integrated monitoring of irradiance, electrical variables, and panel angle. These studies demonstrate practical feasibility across different configurations, but their capacities, operating conditions, control structures, and evaluation measures are not directly comparable. Asyari and Aji (2023) likewise reported an Arduino- and LDR-based dual-axis configuration, reinforcing the need for comparable reporting of control assumptions and energy boundaries.

Mechanical and net-energy considerations are especially important at small panel capacities. Wendryanto et al. (2017) addressed a two-axis drive mechanism, Widjonarko et al. (2024) reported improved performance for a 50 Wp tracking system, and Prasetiyo et al. (2022) emphasized that generated energy should be evaluated against drive-system consumption. Hidayah and Irawan (2024) further illustrated the potential of adaptive control, while also implying a need to balance algorithmic sophistication with controller capability and implementation requirements. Consequently, a useful design-stage study should connect orientation control, mechanical transmission, actuator-energy accounting, and safety logic rather than report gross output alone. International experimental and methodological studies likewise show that comparator geometry, parasitic tracker consumption, and net energy must be reported explicitly rather than inferred from gross panel output alone (Tan et al., 2021; Osman et al., 2022; Shang & Shen, 2023). Field and model-based comparisons further show that energy-yield claims depend strongly on fixed-panel geometry, climate, tracking consumption, and measurement boundaries (Eke & Şentürk, 2012; Koussa et al., 2011; Lazaroiu et al., 2015).

The literature synthesis motivates four design gaps. First, many educational and low-cost prototypes rely on servo motors or open-loop steppers, so rotor following errors may remain undetected. Second, absolute ADC differences can make the control threshold depend on illumination level unless the sensor imbalance is normalized. Third, tracking decisions are not always reported together with homing, bidirectional limit interlocks, driver alarms, emergency shutdown, night parking, and wind-based stow logic. Fourth, gross energy comparisons may omit actuator consumption and therefore overstate the practical benefit of tracking. These gaps are presented as a design rationale for system integration; they do not establish that each individual feature is unprecedented in the international literature.

Table 1. Selective Literature Positioning and Role in the Present Design Rationale

Source(s)	Emphasis reported in the cited literature	Role in the present manuscript
Awasthi et al. (2020); Fuentes-Morales et al. (2020)	Reviews of solar-tracking technologies and control algorithms.	Provide the international control landscape and the basis for distinguishing open-loop, sensor-based, and hybrid strategies.
Jamroen et al. (2020)	Low-cost dual-axis tracking based on digital logic and implementation.	Supports the use of low-cost directional sensing while motivating explicit filtering, deadband, and implementation constraints.
Asmi and Candra (2020); Hakim and Sukma (2022)	Arduino-, LDR-, and stepper-based dual-axis prototypes.	Motivate the selected controller and sensing architecture; the present study adds a layered supervisory design and explicit evidence boundaries.

Source(s)	Emphasis reported in the cited literature	Role in the present manuscript
Dewanto et al. (2022); Hidayah and Irawan (2024)	Sensor configuration, tracking delay, and adaptive/fuzzy control.	Motivate analysis of tuning, response delay, controller complexity, and actuator-movement trade-offs.
Prasetiyo et al. (2022); Widjonarko et al. (2024)	Energy comparison and implementation, including a 50 Wp configuration.	Motivate same-capacity comparison and explicit subtraction of modelled actuator energy from gross gain.
Wendryanto et al. (2017); Pardosi et al. (2024); Soedjangi (2025)	Mechanical drive development, Arduino implementation, and monitored operating variables.	Demonstrate practical design interest while highlighting the need for consistent reporting of mechanics, control, safety, and measurement boundaries.
Tan et al. (2021); Osman et al. (2022)	Methodological and experimental evaluation of parasitic tracker consumption and net energy yield.	Strengthen the requirement to define the complete tracker-energy boundary and to distinguish gross from net benefit.
Shang and Shen (2023); Mamodiya and Tiwari (2023)	Physical dual-axis implementations and comparison of control strategies.	Provide external benchmarks for prototype validation and motivate direct comparison with alternative controller architectures.

The proposed design uses a 50 Wp panel, an Arduino Mega 2560, four LDRs with a cross shade, an RTC DS3231, two 3 N·m closed-loop NEMA 23 motors, two 24-48 V drivers, a 20:1 worm gearbox, and a 20T:60T timing-pulley transmission. The theoretical total reduction ratio is 60:1. The structure is specified with a 20 mm solid-steel shaft, UCP204 pillow blocks, a 30 × 30 × 2 mm hollow secondary frame, and a 50 × 50 × 2.3 mm main frame. These component values are design specifications; they have not been validated through a completed physical build, load test, or wind-load test.

The contribution of this study is system-level integration rather than a new tracking algorithm. The orientation layer converts normalized LDR imbalance into azimuth and elevation corrections through filtering, a deadband, and dominant-axis scheduling. The actuator layer uses driver-side encoder feedback to reduce rotor following error. The supervisory layer defines INIT, HOMING, TRACKING, HOLD, PARK, STOW, and FAULT modes with safety priority, wind hysteresis, and manual reset. The transferable contribution is the explicit separation of orientation control, rotor control, supervisory safety logic, energy accounting, and the evidence required before model outputs can be treated as hardware performance.

Transferable Design Principles

The system-level contribution is operationalized through five transferable design principles: (1) separate panel-orientation sensing from motor-rotor following control; (2) give supervisory safety states priority over energy-maximizing states; (3) evaluate gross photovoltaic gain together with parasitic tracker consumption; (4) label every reported output according to its evidence level, distinguishing design specifications, model residuals, scenario estimates, expected state responses, and measured hardware performance; and (5) re-parameterize geometry, control tuning, wind thresholds, and fixed-panel orientation for each site and panel scale. These principles are proposed engineering design propositions and have not yet been validated as general laws through comparative experiments.

Scope and Intended Educational Use

The manuscript is an engineering design and simulation study, not an empirical educational intervention. Its potential educational value lies in serving as a laboratory case for teaching mechatronic integration, hierarchical control, renewable-energy measurement, and safety-by-design. No students, instructors, learning outcomes, curriculum implementation, or pedagogical effectiveness were evaluated; therefore, the study does not claim evidence of educational impact. Its proposed laboratory use is consistent with evidence that inductive, project-based, and experiential approaches can support engineering learning when activities, assessment, and outcomes are explicitly aligned (Prince & Felder, 2006; Servant-Miklos & Kolmos, 2022; Tembrevilla et al., 2024).

Proposed Educational Laboratory Application

A prospective laboratory application can be organized in four stages. Stage 1 requires learners to map the mechanical, electrical, sensing, control, and safety subsystems and identify interfaces and failure points. Stage 2 requires implementation or inspection of normalized LDR error, filtering, deadband, dominant-axis scheduling, and the supervisory state machine. Stage 3 requires calibration planning, matched-panel comparison, energy-boundary definition, and uncertainty reporting. Stage 4 requires scenario-based fault injection and a technical justification of PARK, STOW, and FAULT priorities. Expected student artifacts would include an architecture diagram, controller pseudocode, a parameter and data dictionary, a verification matrix, an energy balance, and a reflective engineering report. This is a proposed instructional use only; participants, instructional implementation, assessment validity, and learning outcomes were not studied. The sequence is intentionally problem- and project-oriented, but its educational effectiveness must be tested rather than assumed (Prince & Felder, 2006; Servant-Miklos & Kolmos, 2022).

Any future educational evaluation should specify the learner population, course context, learning objectives, instructional duration, assessment rubrics, evidence of instrument validity and reliability, comparison or baseline conditions where appropriate, data-protection procedures, and research-ethics approval. Until such evidence is available, the manuscript supports use as a design case rather than a demonstrated educational intervention.

This study aims to specify and evaluate a simulation-based design framework for a dual-axis solar tracker for a 50 Wp panel. It addresses four research questions: (RQ1) How can the mechanical, sensing, actuation, control, and safety subsystems be integrated into one hierarchical architecture? (RQ2) Under the prescribed deterministic scenario, what modelled panel energy, residual tracking error, actuator-energy estimate, and net-energy estimate are produced? (RQ3) Does the state-machine logic generate the expected priority transitions under injected operating and fault conditions? (RQ4) Which uncertainties and validation steps must be resolved before the results can be transferred to a physical prototype, another location, or an educational laboratory?

METHOD

This study uses an engineering-design approach with quantitative evaluation through deterministic simulation. The system is divided into mechanical, power-electronics, sensor-acquisition, tracking-control, and safety subsystems. Two model configurations were compared under the same prescribed irradiance and temperature profiles: a panel with the proposed dual-axis tracker and a fixed comparator. The schedule from 08:00 to 17:00 contains ten hourly reporting points per day and nine one-hour trapezoidal integration intervals per day. Across seven days, this produced 70 reported observations for each configuration. The seven days are deterministic scenario cases rather than a random sample from a defined population.

Simulation Scope, Inputs, and Reproducibility Boundaries

The original design record did not provide the simulation software and version, executable code, geographic coordinates, calendar dates, a site-specific solar-position routine, or the complete high-frequency input series. The present revision therefore does not claim full computational reproducibility or location-specific prediction. Irradiance, panel-temperature, wind-speed, and target-orientation series should be interpreted as prescribed design-stage inputs. Independent replication requires release of the complete input data, parameter file, controller pseudocode or source code, numerical time step, software environment, and fixed-panel geometry. Until those materials are supplied, the tabulated results can be checked for internal arithmetic consistency but cannot be independently regenerated in full. These disclosures follow established expectations for reproducible computational research, including accessible code, complete inputs, explicit parameters, and traceable analysis steps (Sandve et al., 2013).

The Arduino Mega 2560 is specified as the supervisory controller. Its input set comprises four LDRs, the RTC DS3231, an anemometer, four normally closed limit switches, emergency-stop status, and alarms from both motor drivers; its outputs are STEP, DIR, and ENABLE signals for each axis. The model variables include irradiance, panel temperature, wind speed, target and modelled azimuth, target and modelled elevation, LDR ADC values, normalized errors, active state, voltage, current, panel power, motor-active duration, alarms, and actuator energy. In a reproducible implementation, each variable should be logged with its unit, sampling interval, and source or calculation rule.

The proposed electrical architecture separates the actuator-power line from the logic line. The two motor drivers receive a nominal 36 V supply, whereas the Arduino, RTC, sensors, and data-logging circuit receive 5 V from an isolated converter. The design uses a controlled ground reference or isolators for STEP, DIR, ENABLE, and alarm signals according to driver requirements. The emergency stop is placed on the hardware enable or actuator-power path so that shutdown does not depend on program execution. Encoder, anemometer, and LDR wiring is specified separately from motor wiring, with shielding or twisted pairs for long runs. These are design provisions for signal integrity and fail-safe behavior; electromagnetic compatibility and hardware response were not experimentally tested.

The conceptual mechanical structure uses a 50 × 50 × 2.3 mm hollow-steel main frame and a 30 × 30 × 2 mm secondary frame. The panel is mounted on a 20 mm solid-steel shaft supported by UCP204 pillow blocks. The elevation axis is positioned near the assumed panel center of mass, while the azimuth axis rotates the upper assembly. This arrangement is intended to reduce static gravitational moment and bearing load, but the present study does not include finite-element analysis, measured center-of-gravity data, fabrication tolerance, or physical deflection testing.

Each axis is specified with a 3 N·m closed-loop NEMA 23 motor, a 24-48 V driver rated at a minimum of 4.2 A per phase, a 20:1 worm gearbox, and a 20T:60T timing pulley. The 3:1 pulley ratio gives a theoretical total reduction of 60:1, and a 1.8° motor full step corresponds to an ideal command increment of 0.03° at the output shaft. This value is command resolution, not demonstrated panel accuracy. A complete sizing assessment still requires panel mass, center of gravity, friction, gearbox and belt efficiency, acceleration, shaft and bearing loads, aerodynamic wind moment, stow load, and appropriate safety factors. Consequently, the selected ratings are provisional design choices rather than evidence of mechanical feasibility.

The outer orientation loop uses four LDRs in the left-upper (LU), right-upper (RU), left-lower (LD), and right-lower (RD) quadrants. The side intensities are defined as $S_L = L_{LU} + L_{LD}$, $S_R = L_{RU} + L_{RD}$, $S_U = L_{LU} + L_{RU}$, and $S_D = L_{LD} + L_{RD}$. The normalized errors reduce direct dependence on absolute illumination. The constant ε is a small positive denominator guard used to prevent division by zero under very low light; its numerical value must be reported in any reproducibility package.

$$e_{az} = (S_L - S_R) / (S_L + S_R + \varepsilon)$$
$$e_{el} = (S_U - S_D) / (S_U + S_D + \varepsilon)$$

LDR readings are processed with an eight-sample moving average. The design deadband is stated as equivalent to approximately 0.5°; however, no physical calibration curve between normalized LDR imbalance and panel angle is available in the submitted record. In each one-second control cycle, the controller first evaluates safety inputs, then calculates both normalized errors. If both remain within the deadband, the logic enters HOLD and suppresses pulses. If one error exceeds the deadband, the axis with the larger absolute error receives a bounded STEP/DIR burst. The intended non-blocking sequence is: read interlocks and alarms; determine FAULT/STOW/PARK priority; acquire and filter LDR values; compute normalized errors; select HOLD or the dominant axis; issue a limited pulse burst; update the modelled position and log the event; and return to the safety checks. This sequence is a design specification and should be accompanied by executable code or detailed pseudocode in a reproducibility supplement.

The inner loop is located in each closed-loop driver. The motor encoder compares rotor position with command pulses, after which the driver regulates phase current to reduce rotor following error and identify missed-step conditions. After homing, nominal position is derived from the encoder and step counter. The motor-side encoder does not measure gearbox backlash, belt slip, joint looseness, or structural deflection downstream of the motor shaft. Therefore, the reported simulation residuals are not equivalent to independently measured panel-angle accuracy. Prototype validation requires an inclinometer or absolute encoder on the output shaft so that rotor following error can be separated from panel-orientation error.

The supervisory state machine consists of INIT, HOMING, TRACKING, HOLD, PARK, STOW, and FAULT. INIT checks communications, sensors, and driver status; HOMING searches for reference limits and establishes the model zero. TRACKING generates corrections when a normalized error exceeds the deadband, whereas HOLD stops pulses when the orientation criterion is satisfied. PARK is selected outside 08:00-17:00 or under low-light conditions. STOW overrides tracking at wind speed ≥12 m/s and commands initial targets of 0° azimuth and 5° elevation. Recovery is permitted only at wind speed ≤10 m/s after 60 s of stability. These thresholds are design assumptions and require validation against structural capacity, panel geometry, local gust characteristics, and applicable safety standards. Hierarchical and hybrid solar-tracking studies similarly emphasize explicit control priorities, mode transitions, and the distinction between sensor-driven and calculated-position strategies (Rubio et al., 2007; Yao et al., 2014).

FAULT is specified for an active emergency stop, a driver alarm, simultaneous activation of two limits on one axis, or a homing timeout. The expected response is to stop STEP pulses, disable ENABLE, store a fault code, and require manual reset. The emergency stop also interrupts the actuator enable or power path through hardware, and normally closed limit contacts are intended to make cable discontinuity detectable. The RTC provides timestamps, defines the operating window, and initiates PARK. These responses are evaluated as logical state transitions only; hardware cutoff time, relay or driver failure modes, and standards compliance were not measured.

The panel-power model is reported as $P = P_{STC}(G/1000)[1 + \gamma(T_p - 25)]\eta_s F_{or}$, where P_{STC} = 50 Wp, G is irradiance (W/m²), T_p is panel temperature (°C), γ = -0.004/°C, η_s = 0.96, and F_{or} is the prescribed orientation multiplier. The submitted design record does not provide a location-specific incidence-angle equation, exact fixed-panel tilt and azimuth, solar

coordinates, or a component-level justification for η_s. Thus, F_{or} and η_s should be treated as scenario assumptions rather than validated site parameters. Daily energy is calculated by trapezoidal integration across nine one-hour intervals. Gross gain is $(E_{tracker} - E_{fixed})/E_{fixed} \times 100\%$, and estimated net gain is $E_{tracker} - E_{fixed} - E_{motor}$. A reproducible site-specific implementation should calculate solar position using a documented algorithm and should justify temperature-related power corrections with established photovoltaic performance relationships (Reda & Andreas, 2004; Skoplaki & Palyvos, 2009).
Control performance is summarized using mean absolute error (MAE), root mean square error (RMSE), and maximum residual error for azimuth and elevation. Panel energy is reported as daily values, seven-day totals, descriptive mean, standard deviation, and range. Because the seven days are deterministic cases rather than independent random observations, inferential confidence intervals are not used in the revised interpretation. The actuator-energy value is a model estimate derived from scheduled motor-active duration. The submitted record does not provide current time series, acceleration/deceleration profiles, driver losses, gearbox and belt efficiencies, holding-current behavior, or auxiliary consumption by the controller and sensors. The resulting net-energy estimate should therefore be regarded as an optimistic design-stage value. No formal sensitivity, Monte Carlo, or uncertainty-propagation analysis was performed. Because model outputs are assumption-dependent, future uncertainty analysis should follow transparent sensitivity-analysis practices rather than vary parameters without a defined design or interpretation framework (Saltelli et al., 2019).

Residual and Energy-Metric Definitions

$$r_{az,t} = \theta_{az,target,t} - \theta_{az,model,t}$$
$$r_{el,t} = \theta_{el,target,t} - \theta_{el,model,t}$$
$$MAE_{axis} = (1/n)\ \Sigma(t=1 \text{ to } n)\ |r_{axis,t}|$$
$$RMSE_{axis} = \sqrt{[(1/n)\ \Sigma(t=1 \text{ to } n)\ r_{axis,t}^2]}$$
$$E_{act} = (1/3600)\ \Sigma(t=1 \text{ to } m)\ V_{m,t}\ I_{m,t}\ \Delta t_t$$

Here, r is the difference between the prescribed target angle and the modelled angle; n denotes the reported residual observations used for each axis summary, and the seven-day record contains 70 hourly reporting points per configuration. E_{act} is the auditable electrical-energy form for the actuator path, where $V_{m,t}$ and $I_{m,t}$ are motor-system voltage and current over interval Δt_t. The submitted record does not contain the underlying target-angle series, modelled-angle series, voltage-current time series, or high-frequency motor-event log. Consequently, the published MAE/RMSE and 0.495 Wh/day actuator value can be checked only as reported aggregates and cannot be independently recalculated from the manuscript.

Verification Criteria and Evidence Boundary

The deterministic logic checks use predefined acceptance targets: the modelled combined RMSE is below 0.5°; commands do not proceed farther into an active limit; a driver alarm or emergency condition terminates pulses; STOW has priority over tracking; and recovery requires the defined hysteresis and time delay. These checks establish expected software-state behavior only. The submitted record does not include a complete event log, repeated trials, response-latency distribution, concurrent-fault matrix, or independent sensor reference. A prototype test plan should report initial state, injected condition, expected state, observed state, transition latency, command output, final angle, energy use, and fault-code result for each repeated scenario.

Table 2. Main Components, Control Architecture, and Simulation Boundaries

Component/parameter	Specification
Photovoltaic panel	50 Wp tracker model and one fixed-comparator model; exact site-specific fixed tilt/azimuth not provided
Controller	Arduino Mega 2560, 16 MHz
Direction sensor	Four LDRs with cross shade; normalized azimuth and elevation errors
Actuators	Two closed-loop NEMA 23 motors, 3 N·m
Transmission	20:1 worm gearbox and 20T:60T pulley; total reduction 60:1
Actuator supply	36 V; 24–48 V driver, ≥4.2 A/phase
Control method	8-sample moving average; deadband equivalent to 0.5°; STEP/DIR burst; dominant-axis priority
Protection	Four NC limit switches, anemometer, hardware E-stop, driver alarms, and homing timeout
Mechanical structure	Ø20 mm steel shaft; UCP204; 30×30×2 and 50×50×2.3 mm hollow sections
Simulation schedule	Seven deterministic days; 08:00-17:00 inclusive; ten hourly reporting points and nine integration intervals per day
State machine	INIT, HOMING, TRACKING, HOLD, PARK, STOW, and FAULT
Wind logic	STOW at ≥12 m/s; recovery at ≤10 m/s after 60 s of stability
STOW target	0° azimuth and 5° elevation; tracking is canceled during high-wind conditions
Control cycle	1 s design cycle; non-blocking logic; hourly reporting summary
Study status	Simulation-based design; no physical prototype or field data
Environmental basis	Prescribed irradiance, temperature, and wind scenarios; no documented geolocation, season, or random sampling
Energy-model boundary	Orientation multiplier and η_s are scenario assumptions; no MPPT dynamics, auxiliary electronics, ageing, or full conversion-loss model
Uncertainty analysis	Descriptive statistics only; no inferential confidence interval, sensitivity analysis, Monte Carlo analysis, or uncertainty propagation
Reproducibility package	Software, code, complete inputs, and parameter file were not supplied with the submitted manuscript

Table 3. Evidence Classification and Permissible Claim Boundaries

Domain	**Evidence available in the manuscript**	**Status and permissible interpretation**	**Evidence required for transfer**
System architecture	Component specifications, block diagrams, control sequence, and state definitions.	Proposed design specification; supports discussion of intended integration only.	Prototype construction, interface verification, and configuration-controlled documentation.
Photovoltaic energy	Seven prescribed daily aggregates generated under an incompletely documented model.	Scenario estimate; supports arithmetic comparison only under the stated assumptions.	Complete inputs, solar geometry, fixed-panel orientation, MPPT/load model, sensitivity analysis, and field measurements.
Tracking performance	Model-target residual summaries and an imposed 0.5° design threshold.	Internal model check; does not establish output-shaft or panel-angle accuracy.	Independent angle sensor, calibration curve, repeated approaches, backlash and uncertainty analysis.
Safety logic	Priority rules and expected deterministic responses to injected logical conditions.	Software-state expectation; does not establish certified or measured safe operation.	Event logs, transition latency, concurrent-fault tests, hardware cutoff measurement, hazard analysis, and standards assessment.
Practical and educational use	Conceptual transfer requirements and a proposed laboratory sequence.	Prospective application only; no economic, operational, or learning-effect claim is supported.	Bill of materials, lifecycle and environmental tests, and a separate educational study with validated assessments.

Figure 1. Conceptual Mechanical Design of the Proposed 50 Wp Dual-Axis Tracker

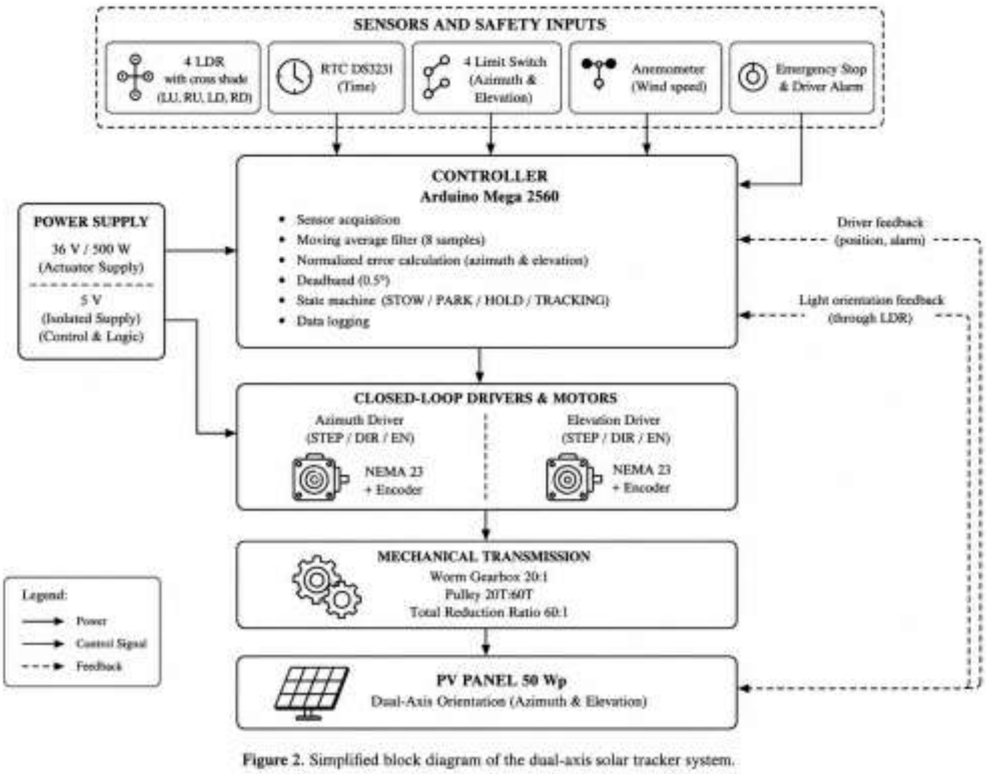

Figure 2. Proposed Hierarchical Control Architecture of the 50 Wp Dual-Axis Tracker

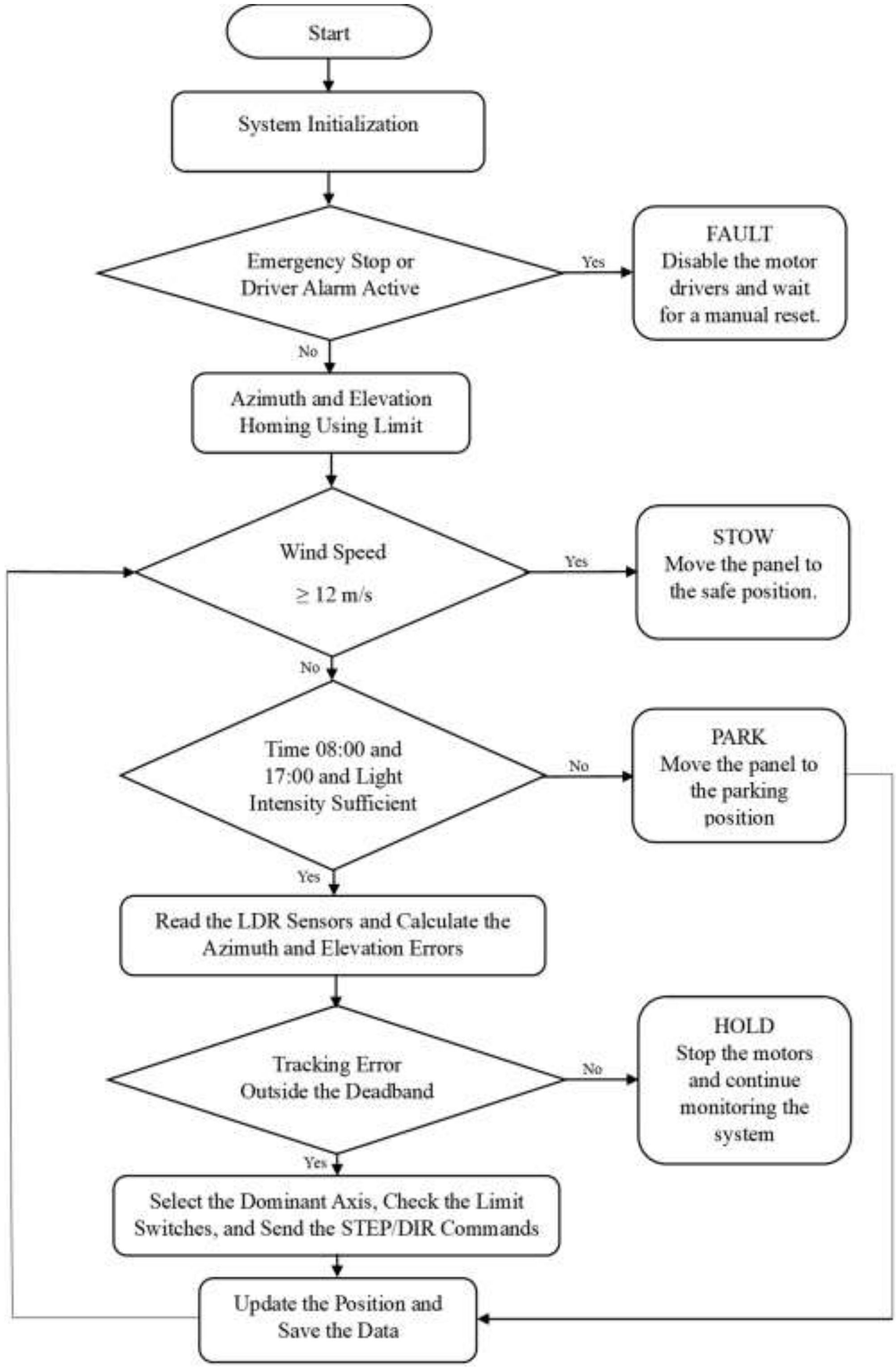

Figure 3. Proposed Supervisory State-Machine Flow for Tracking, Parking, Stow, and Fault Handling

RESULTS AND DISCUSSION

Photovoltaic Energy Performance

Figure 4 presents the mean hourly modelled output power across the seven prescribed days. Both configurations follow the imposed irradiance pattern, increasing toward midday and decreasing in the afternoon. The tracker model reaches 40.41 W at 12:00 and the fixed-comparator model reaches 38.37 W. The smaller midday difference is consistent with a fixed panel receiving a more favorable incidence angle around solar noon, whereas the prescribed orientation advantage of tracking is larger in the morning and afternoon. These values are scenario outputs and are not measurements from a field installation.

Energy integrates the hourly power profile. Figure 5 and Table 4 report tracker-model energy of 230.45-310.71 Wh/day and fixed-comparator energy of 195.13-261.38 Wh/day. Day-to-day differences follow the prescribed irradiance and panel-temperature inputs. Applying the same environmental inputs to each paired configuration supports an internally controlled model comparison, but it does not remove uncertainty associated with the undefined site, fixed-panel geometry, orientation multiplier, electrical-load assumptions, or model simplifications.

The descriptive mean is 283.93 Wh/day for the tracker model and 237.48 Wh/day for the fixed comparator. The mean percentage gain is 19.56%, with a descriptive standard deviation of 1.13% and a seven-day range of 18.10-21.41%. The seven-day totals are 1,987.50 Wh and 1,662.36 Wh, respectively. Because the days are deterministic scenario cases, these statistics summarize variation among the prescribed inputs; they do not estimate sampling uncertainty or support population-level inference.

The magnitude of the simulated gain is broadly compatible with the direction of findings reported for other tracking systems, including a 50 Wp implementation by Widjonarko et al. (2024), higher output from an Arduino-based system by Pardosi et al. (2024), and energy benefits reported by Prasetiyo et al. (2022). Nevertheless, direct numerical benchmarking is not valid because panel capacity, fixed orientation, latitude, season, weather, electrical loading, sampling interval, and actuator-energy boundaries differ across studies. The present result should therefore be interpreted as internal model consistency rather than external validation.

Experimental publications using physical tracking systems provide a more demanding benchmark because they define comparator orientation, control hardware, and measured energy boundaries (Osman et al., 2022; Shang & Shen, 2023). Comparative control research also shows that conclusions depend on the selected strategy and test environment (Mamodiya & Tiwari, 2023). The present model cannot be numerically ranked against those systems because the site, geometry, complete input series, and electrical boundary are not available. The literature is therefore used to define validation requirements, not to claim equivalent or superior performance. Additional fixed-versus-tracking studies illustrate that reported gains vary with environmental conditions and the treatment of tracker consumption (Eke & Şentürk, 2012; Koussa et al., 2011; Lazaroiu et al., 2015; Yao et al., 2014).

The morning and afternoon advantage results from the prescribed reduction in angular mismatch, while the smaller noon advantage reflects the favorable noon orientation of the fixed comparator. Underperformance would be expected when diffuse irradiance dominates, LDRs are unevenly shaded, calibration drifts, the fixed panel is already optimally oriented, frequent corrections increase actuator use, or wind events force extended STOW periods. Transfer to another site requires explicit latitude, season, solar geometry, fixed-panel tilt and azimuth, local wind regime, and identical electrical loading. Prototype comparison should use matched panels, simultaneous measurement, the same MPPT or load, calibrated voltage and current sensors, and a documented uncertainty budget.

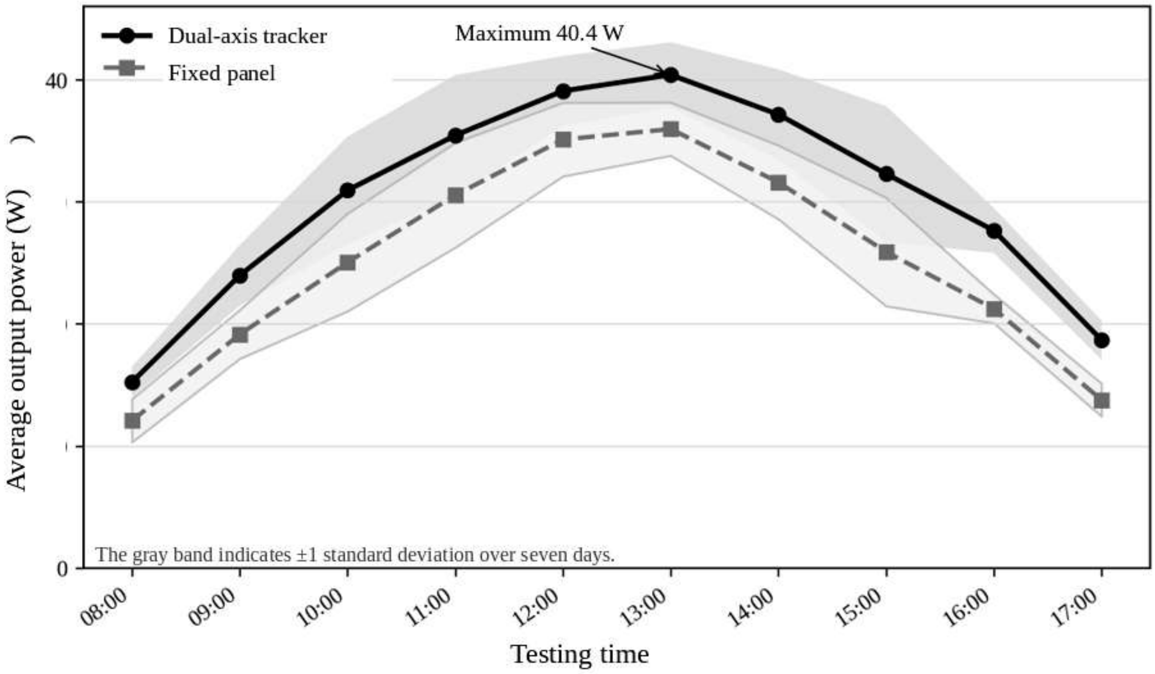

Figure 4. Mean Hourly Modelled Output Power of the Tracked and Fixed 50 Wp Configurations

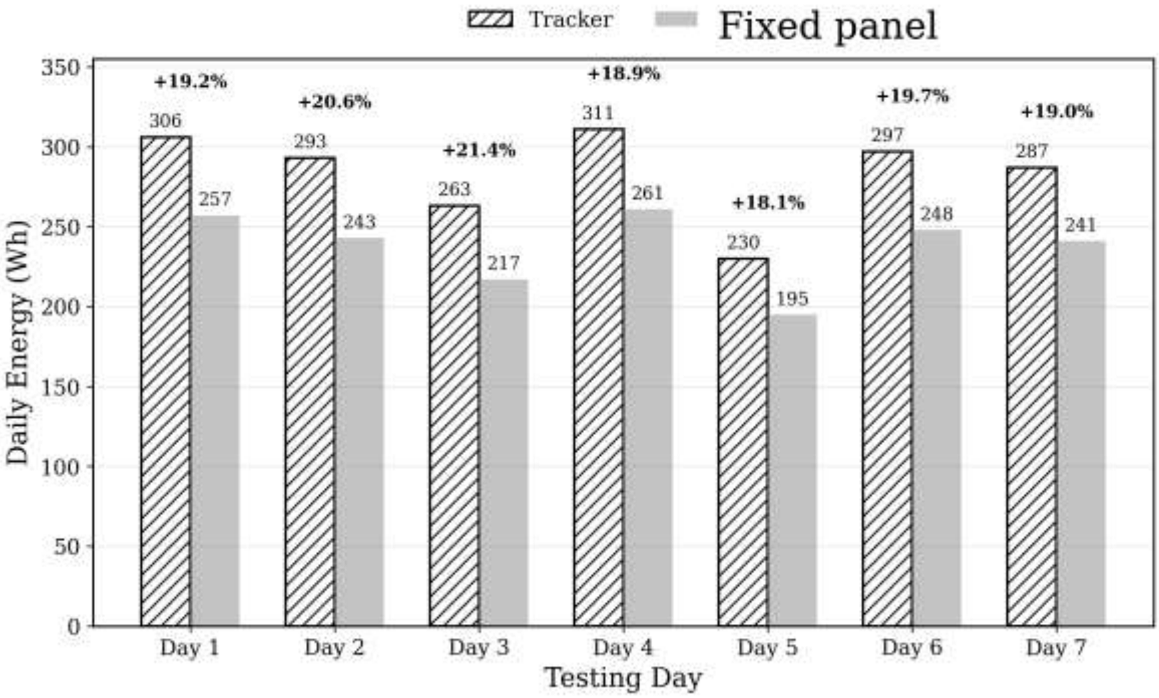

Figure 5. Daily Modelled Energy and Percentage Gain across Seven Prescribed Days

Table 4. Daily Simulated Energy, Estimated Actuator Consumption, and Estimated Net Gain

Day	Tracker (Wh)	Fixed (Wh)	Gain (%)	Estimated actuator energy (Wh)	Estimated net gain (Wh)
Day 1	306.41	257.14	19.16	0.487	48.78

Day	Tracker (Wh)	Fixed (Wh)	Gain (%)	Estimated actuator energy (Wh)	Estimated net gain (Wh)
Day 2	292.89	242.77	20.65	0.490	49.63
Day 3	262.91	216.54	21.41	0.489	45.88
Day 4	310.71	261.38	18.87	0.487	48.84
Day 5	230.45	195.13	18.10	0.494	34.83
Day 6	297.26	248.36	19.69	0.539	48.37
Day 7	286.87	241.04	19.01	0.478	45.35
Average	283.93	237.48	19.56	0.495	45.95

Control-System Design and Tracking Performance

Figure 2 separates the proposed control architecture into an LDR-based orientation loop, driver-side rotor-position loops, supervisory logic, and mechanical transmission. The Arduino performs filtering, normalization, state selection, STEP/DIR generation, event logging, and interlocking. This distinction is important because the LDRs estimate directional imbalance relative to incident light, whereas the encoders verify rotor response to commanded pulses. Neither signal independently measures the final panel angle after the gearbox, pulley, shaft, and frame.

Figure 3 specifies the intended supervisory sequence. Each cycle checks the emergency stop, driver alarms, limits, wind, time, LDRs, and modelled position before issuing a correction. FAULT and STOW are evaluated before PARK and TRACKING/HOLD. Dominant-axis scheduling limits simultaneous motor commands and can reduce current peaks and mechanical interaction, but its comparative advantage was not tested against simultaneous-axis, open-loop solar-position, or hybrid control. Such benchmarking is required before claiming superior robustness or efficiency.

Figure 6 and Table 5 summarize model-residual error rather than independently measured panel-angle accuracy. The mean azimuth MAE is 0.139° and the mean elevation MAE is 0.116°; the corresponding RMSE values are 0.170° and 0.145°, with a combined RMSE of 0.158°. The maximum model residual is 0.44°. These small values show that the idealized command-and-response model remains within the imposed 0.5° evaluation threshold, but they may be partly determined by the assumed kinematics, deadband, and absence of measured backlash, sensor uncertainty, and structural deformation.

The design-stage acceptance targets are a combined model RMSE below 0.5°, no command farther into an active limit, no nominal driver-following alarm, and transfer of each injected safety condition to the expected state within one nominal control cycle. The 0.158° residual provides numerical margin relative to the model threshold; it does not establish physical repeatability. Hardware evaluation should include at least 30 repeated approaches from both directions, an independent output-shaft angle reference, and reporting of mean error, dispersion, backlash, hysteresis, overshoot, settling time, and failure events.

The model residual rises slightly during lower-irradiance periods, which is consistent with reduced LDR signal-to-noise ratio. Normalization can reduce dependence on absolute intensity and the moving average can suppress short fluctuations, but filtering also adds delay. A smaller deadband may improve model alignment while increasing movement frequency and energy consumption; a larger deadband reduces corrections but increases orientation error. A future sensitivity experiment should vary filter length, sampling interval, deadband, burst size, and low-light threshold, and should evaluate residual error, response time, correction count, actuator energy, and fault-detection latency.

The ideal 0.03° command increment is smaller than the simulated RMSE, indicating that command resolution is not the only limiting factor. In a physical system, gearbox backlash, belt compliance, joint looseness, encoder mounting, sensor calibration, wind loading, and frame deflection can dominate the output-angle error. Closed-loop stepper control verifies rotor response but does not automatically guarantee panel orientation. Relative to an open-loop solar-position controller, an LDR loop can compensate for local optical misalignment but is more vulnerable to shading and diffuse light; a hybrid controller may improve robustness at the cost of additional software, calibration, and failure modes (Awasthi et al., 2020; Fuentes-Morales et al., 2020). Comparative control studies also indicate that the merits of photoelectric, calculated-position, and hybrid strategies must be judged under common test conditions (Hafez et al., 2018; Rubio et al., 2007; Yao et al., 2014).

Benchmarking Requirements

A publishable comparison of dominant-axis scheduling should test at least three controller configurations under identical inputs and hardware assumptions: simultaneous two-axis sensor control, open-loop solar-position control, and a hybrid controller. Outcomes should include angular error, response time, number and duration of movements, peak and cumulative electrical consumption, low-light robustness, shading sensitivity, limit and fault events, and computational burden. Because this comparison was not performed, dominant-axis scheduling is retained as a design hypothesis intended to reduce simultaneous current demand and mechanical interaction, not as a demonstrated superior strategy.

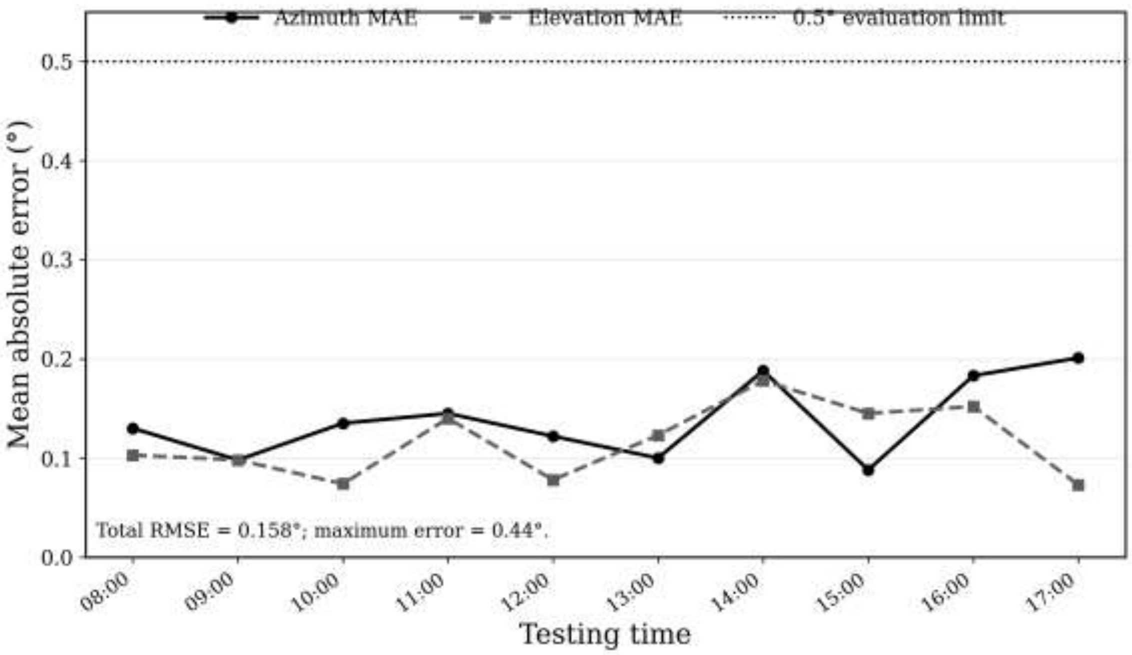

Figure 6. Hourly Model-Residual Mean Absolute Error of the Azimuth and Elevation Loops

Table 5. Simulated Model-Residual Tracking Metrics

Axis	MAE (°)	RMSE (°)	Maximum (°)
Azimuth	0.139	0.170	0.44
Elevation	0.116	0.145	0.39
Combined	0.127	0.158	0.44

Supervisory Control, Actuator Energy, and Safety Performance

The proposed supervisory priority is Emergency/FAULT > STOW > limit interlock > PARK > TRACKING/HOLD. HOMING must be completed before tracking is enabled. TRACKING is selected when one normalized error exceeds the deadband, HOLD when both errors satisfy the threshold, PARK after the operating period or under low light, and STOW when wind reaches the specified trigger. FAULT and emergency conditions require manual reset. This hierarchy is a logical safety design; it is not a certified safety function and has not been validated for hardware timing, single-point failures, or compliance with electrical and machinery standards.

The modelled actuator-energy estimate is 0.495 Wh/day. Relative to the gross additional modelled panel energy of 46.45 Wh/day, this is approximately 1.07%, leaving an estimated net gain of 45.95 Wh/day in Table 4. The estimate is optimistic because the submitted record does not provide motor-current waveforms, acceleration and deceleration, driver losses, gearbox and belt efficiency, holding-current behavior, controller and sensor consumption, or standby power. The value should be labelled as a scenario estimate rather than measured consumption, and a prototype study should use direct electrical measurement of the complete tracker subsystem.

Figure 7 presents the prescribed wind-speed profile and the 12 m/s STOW threshold. One model event on Day 6 at 17:00 reaches 12.8 m/s. Because 17:00 is also the PARK boundary, this event does not isolate STOW priority from time-based parking. It demonstrates the intended logic path only. A stronger verification set should include high-wind events during normal tracking hours, gusts that cross and recross the thresholds, sensor dropout, simultaneous limit and wind events, power interruption, and repeated recovery tests with measured transition latency.

Table 6 summarizes modes, triggers, and expected deterministic responses. The revised wording avoids treating a programmed state transition as proof of physical safety. Normally closed limits are specified as directional interlocks: movement toward an active limit is blocked while movement away remains possible; a two-limit conflict routes the logic to FAULT. Driver alarms and emergency input are expected to terminate pulses and disable the actuator path. These are requirements for prototype verification, not measured outcomes.

Scenario injection was used as a design-stage logic check. The intended cases include homing from multiple initial states, limits in both directions, driver alarm and emergency input during movement, wind above and below the hysteresis thresholds, time transitions across the operating window, and LDR values inside and outside the deadband. The submitted record does not provide a complete event log, repetition count, observed latency, concurrent-event matrix, or failure rate. Therefore, Table 6 reports expected deterministic responses rather than validated pass/fail performance.

The principal practical contribution is the explicit integration of normalization, filtering, deadband control, driver-side feedback, homing, bidirectional limits, wind hysteresis, time-based parking, hardware shutdown, fault coding, and actuator-energy accounting in one design framework. The architecture may also serve as a mechatronics laboratory case in which students examine trade-offs among sensing, control accuracy, correction frequency, energy use, and safe-state behavior. Such educational use remains prospective and requires a separate pedagogical study before any learning-effect claim can be made. As an educational case, the design should therefore be implemented through aligned learning tasks, authentic engineering decisions, and validated assessment rather than through hardware demonstration alone (Prince & Felder, 2006; Tembrevilla et al., 2024).

Practical Significance and Transferability

The design has practical promise as a compact prototype architecture, but economic and operational attractiveness has not been established. The submitted record contains no bill of materials, purchase cost, lifecycle cost, maintenance schedule, weatherproofing specification, corrosion-protection plan, manufacturability assessment, or standards-based risk analysis. Transfer to larger panels requires new torque, shaft, bearing, gearbox, wind-load, power-supply, and structural calculations. Transfer to another geographic location requires site-specific solar geometry, seasonal irradiance and temperature, fixed-panel optimization, local wind statistics, environmental protection, and revised PARK/STOW thresholds.

A subsequent practical-readiness report should include a bill of materials and acquisition cost, power-supply sizing, enclosure and ingress-protection rating, corrosion protection for humid or saline environments, maintenance intervals, replaceable components, manufacturability, structural and electrical safety factors, applicable standards, and lifecycle energy and cost. None of these data are available in the present manuscript; accordingly, no claim of affordability, maintainability, economic payback, or deployment readiness is made.

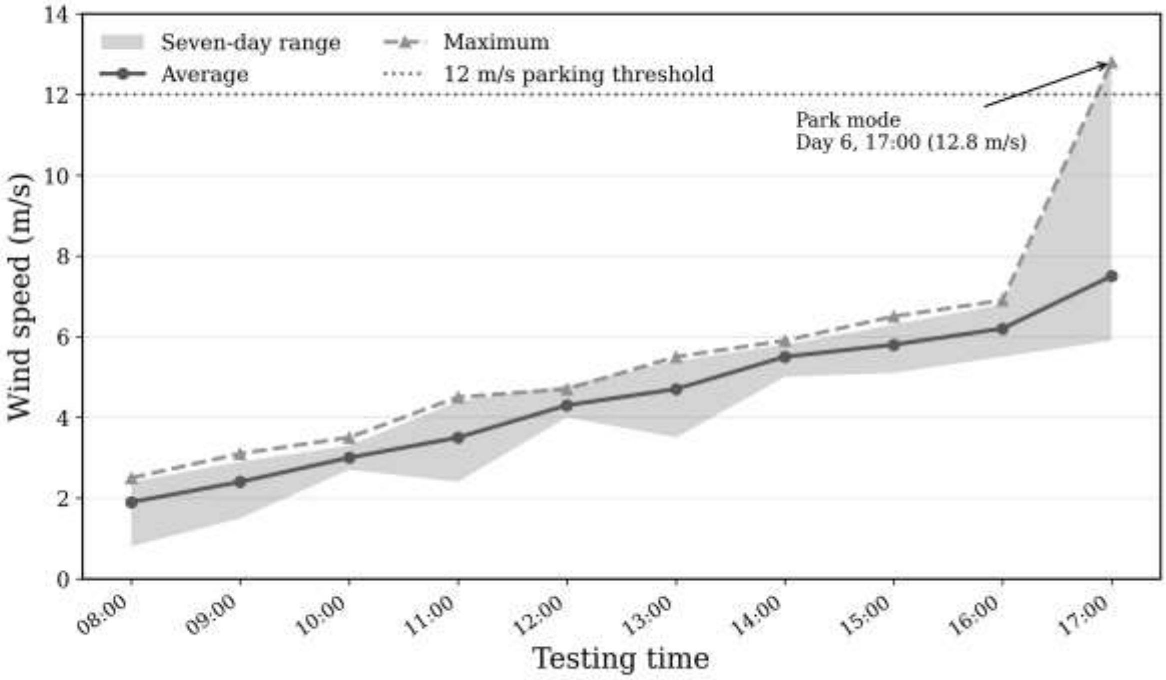

Figure 7. Prescribed Wind-Speed Profile and the 12 m/s Stow Threshold

Table 6. Control Modes, Priority Logic, and Expected Deterministic Responses

Mode/condition	Trigger	Expected deterministic response
INIT	System is powered on	Define initialization of I/O, RTC, drivers, sensors, and logging; hardware timing not measured.
HOMING	Reference position is not yet known	Command motion toward the NC reference limit, set the model zero, and route timeout to FAULT.

Mode/condition	**Trigger**	**Expected deterministic response**
TRACKING	One |e| > deadband	Select the axis with the larger |e| and issue a bounded STEP/DIR burst.
HOLD	Both |e| values are within the deadband	Stop pulses while continuing to check safety and supervisory inputs.
PARK	Outside 08:00–17:00 or under low light	Command the defined night/power-saving position while maintaining interlock monitoring.
STOW	Wind ≥12 m/s	Cancel tracking and command the stated stow targets of 0° azimuth and 5° elevation.
STOW recovery	Wind ≤10 m/s and stable for 60 s	Return to operating-state evaluation only after wind ≤10 m/s for 60 s.
Limit interlock	Movement-direction limit is active	Block movement farther toward the active limit; route a two-limit conflict to FAULT.
Driver fault	Driver alarm is active	Stop STEP, disable ENABLE, store a fault code, and require manual reset.
Emergency	E-stop is active	Interrupt the hardware actuator path and enter highest-priority FAULT.

Integrated Interpretation, Limitations, and Validation Priorities

The deterministic results are internally coherent with the proposed subsystem relationships: the transmission defines ideal command resolution; the LDR model supplies normalized directional imbalance; the controller applies supervisory priority and dominant-axis correction; and the safety inputs restrict commands. The reported 19.56% gain is meaningful only within the prescribed energy model and because the modelled actuator estimate is small. It should not be interpreted as a verified field-energy benefit, economic return, or certified safe response.

The distinction between control cycle and reporting interval is essential. The design specifies a nominal one-second supervisory cycle, whereas research outputs are summarized at ten hourly points from 08:00 to 17:00. In a prototype, safety and state inputs should be evaluated at 0.5-1 s or faster as justified by hazard analysis; LDR acquisition may be faster to form the moving average; and raw data should be logged at a frequency sufficient to resolve motion, fault, and wind transitions. Hourly summaries alone cannot verify emergency-stop latency, limit response, overshoot, or transient energy use.

Prototype testing should use matched 50 Wp panels measured simultaneously under the same load or MPPT conditions. Voltage and current sensors should be calibrated against traceable references, the anemometer against a comparison instrument, and panel angle against an inclinometer or output-shaft encoder. Mechanical testing should include torque margin, backlash, deflection, wind moment, repeated homing, restart after power loss, cable discontinuity, limit conflict, driver alarm, emergency stop, daytime STOW and recovery, and long-duration exposure. Each scenario should report repetition count, latency, final angle, energy use, uncertainty, and any failure event.

The main limitations are the seven-day deterministic scenario, absence of a physical prototype, lack of a documented simulation platform and complete code, unspecified geolocation and season, undefined site-specific fixed-panel orientation, no independent output-angle reference, and incomplete actuator-energy accounting. The model also excludes rain, dust, salt exposure, corrosion, friction variation, belt ageing, gearbox tolerance, structural flexibility, sensor drift and uncertainty, diffuse-light and shadow effects, aerodynamic wind loads, auxiliary electronics consumption, and component failure probabilities. No sensitivity analysis, uncertainty propagation, economic assessment, or standards-compliance evaluation was performed.

The next stage should first make the simulation reproducible by archiving code, software version, all input series, fixed-panel geometry, solar and thermal equations, and parameter values. It should then conduct sensitivity or Monte Carlo analysis to identify assumptions controlling the energy and error results. A physical prototype should subsequently be tested for at least seven documented field days, with simultaneous matched-panel measurements, high-frequency control logs, independent angle measurement, complete tracker-energy measurement, and scenario-based fault testing. If the design is used in education, a separate study should define participants, instructional activities, assessment instruments, learning outcomes, and ethical procedures. Reproducibility and sensitivity analysis should be documented in accordance with established computational-research and model-evaluation guidance (Saltelli et al., 2019; Sandve et al., 2013).

Transparency Statements

Data and code availability: The aggregate values reported in the tables are contained in this manuscript, but the complete input series, executable code, software environment, and high-frequency event logs were not provided with the submitted article. Funding: No funding statement was provided in the submitted manuscript. Conflict of interest: No conflict-of-interest statement was provided in the submitted manuscript. Ethics: The study involved no human or animal participants; research-ethics approval and informed consent were therefore not applicable to the reported simulation.

CONCLUSION

This study specifies a simulation-based design for a dual-axis solar-tracking mechatronic system for a 50 Wp panel. The proposed architecture integrates a steel frame, shaft and bearings, a theoretical 60:1 transmission, two closed-loop NEMA 23 motors, four LDRs, an RTC, an Arduino Mega 2560, modelled energy accounting, hardware-oriented interlocks, and a supervisory state machine covering INIT, HOMING, TRACKING, HOLD, PARK, STOW, and FAULT. Under the prescribed seven-day scenario, the tracker model produced 283.93 Wh/day compared with 237.48 Wh/day for the fixed comparator, corresponding to a descriptive gain of 19.56%. The combined model-residual RMSE was 0.158°, the maximum residual was 0.44°, estimated actuator energy was 0.495 Wh/day, and estimated net gain was 45.95 Wh/day. These outputs support internal consistency of the design framework and provide provisional test targets only. Because the exact simulation environment, site geometry, fixed-panel orientation, full actuator-energy model, independent angle measurement, uncertainty analysis, prototype evidence, economic assessment, and safety certification are absent, the manuscript does not establish physical accuracy, generalizable energy gain, mechanical feasibility, or certified safe operation. Reproducible simulation, sensitivity analysis, prototype construction, matched-panel field testing, independent output-angle measurement, full energy accounting, and repeated fault-scenario verification are required before performance claims can be transferred to practice. Its proposed educational use is limited to a structured mechatronics laboratory case; educational effectiveness remains untested and requires a separate study with participants, validated assessment instruments, ethical procedures, and reported learning outcomes.

REFERENCES

Al-Rousan, N., Isa, N. A. M., & Desa, M. K. M. (2018). Advances in solar photovoltaic tracking systems: A review. *Renewable and Sustainable Energy Reviews*, *82*, 2548–2569. https://doi.org/10.1016/j.rser.2017.09.077

Asmi, J., & Candra, O. (2020). Prototype solar tracker dua sumbu berbasis microcontroller Arduino Nano dengan sensor LDR. *JTEV (Jurnal Teknik Elektro dan Vokasional)*, *6*(2), 54–63. https://doi.org/10.24036/jtev.v6i2.108504

Asyari, H., & Aji, A. W. (2023). Desain solar tracking dual-axis berbasis Arduino dan sensor light dependent resistor untuk meningkatkan daya keluaran sel surya. *JTE UNIBA*, *7*(2), 320–324. https://doi.org/10.36277/jteuniba.v7i2.218

Awasthi, A., Shukla, A. K., Murali Manohar, S. R., Dondariya, C., Shukla, K. N., Porwal, D., & Richhariya, G. (2020). Review on sun tracking technology in solar PV system. *Energy Reports*, *6*, 392–405. https://doi.org/10.1016/j.egyr.2020.02.004

Dewanto, M. R., Priyanto, Y. T. K., Salim, T. D. P., Khatami, M., & Suprapto, S. S. (2022). Perancangan dual-axis solar tracker untuk PLTS dengan analisis pengaruh jumlah sensor dan tracking delay. *Jurnal Sistim Informasi dan Teknologi*, *4*(4), 204–208. https://doi.org/10.37034/jsisfotek.v4i4.181

Eke, R., & Şentürk, A. (2012). Performance comparison of a double-axis sun tracking versus fixed PV system. *Solar Energy*, *86*(9), 2665–2672. https://doi.org/10.1016/j.solener.2012.06.006

Fuentes-Morales, R. F., Diaz-Ponce, A., Peña-Cruz, M. I., Rodrigo, P. M., Valentín-Coronado, L. M., Martell-Chavez, F., & Pineda-Arellano, C. A. (2020). Control algorithms applied to active solar tracking systems: A review. *Solar Energy*, *212*, 203–219. https://doi.org/10.1016/j.solener.2020.10.071

Hafez, A. Z., Yousef, A. M., & Harag, N. M. (2018). Solar tracking systems: Technologies and trackers drive types—A review. *Renewable and Sustainable Energy Reviews*, *91*, 754–782. https://doi.org/10.1016/j.rser.2018.03.094

Hakim, T. D., & Sukma, M. (2022). Rancang bangun dual-axis solar tracker menggunakan mikrokontroler Arduino Mega 2560. *Jurnal Elektro*, *10*(2), 106–118. https://jurnalteknik.unkris.ac.id/index.php/jie/article/view/150

Hidayah, A., & Irawan, D. (2024). Implementasi fuzzy logic pada kontrol solar tracker dual-axis berbasis Haiwel Clouds SCADA. *Techno.Com*, *23*(2). https://doi.org/10.62411/tc.v23i2.10356

Jamroen, C., Komkum, P., Kohsri, S., Himananto, W., Panupintu, S., & Unkat, S. (2020). A low-cost dual-axis solar tracking system based on digital logic design: Design and implementation. *Sustainable Energy Technologies and Assessments*, *37*, 100618. https://doi.org/10.1016/j.seta.2019.100618

Koussa, M., Cheknane, A., Hadji, S., Haddadi, M., & Noureddine, S. (2011). Measured and modelled improvement in solar energy yield from flat plate photovoltaic systems utilizing different tracking systems and under a range of environmental conditions. *Applied Energy*, *88*(5), 1756–1771. https://doi.org/10.1016/j.apenergy.2010.12.002

Lazaroiu, G. C., Longo, M., Roscia, M., & Pagano, M. (2015). Comparative analysis of fixed and sun tracking low power PV systems considering energy consumption. *Energy*

Conversion and Management, *92*, 143–148. https://doi.org/10.1016/j.enconman.2014.12.046

Lee, C.-Y., Chou, P.-C., Chiang, C.-M., & Lin, C.-F. (2009). Sun tracking systems: A review. *Sensors*, *9*(5), 3875–3890. https://doi.org/10.3390/s90503875

Mamodiya, U., & Tiwari, N. (2023). Dual-axis solar tracking system with different control strategies for improved energy efficiency. *Computers & Electrical Engineering*, *111*, 108920. https://doi.org/10.1016/j.compeleceng.2023.108920

Mousazadeh, H., Keyhani, A., Javadi, A., Mobli, H., Abrinia, K., & Sharifi, A. (2009). A review of principle and sun-tracking methods for maximizing solar systems output. *Renewable and Sustainable Energy Reviews*, *13*(8), 1800–1818. https://doi.org/10.1016/j.rser.2009.01.022

Osman, I. S., Almadani, I. K., Hariri, N. G., & Maatallah, T. S. (2022). Experimental investigation and comparison of the net energy yield using control-based solar tracking systems. *International Journal of Photoenergy*, *2022*, 7715214. https://doi.org/10.1155/2022/7715214

Pardosi, C. H., Siregar, M., & Pandjaitan, L. W. (2024). Design and implementation of a dual-axis solar tracking system using Arduino Uno microcontroller. *Jurnal ELTIKOM*, *8*(1), 44–56. https://doi.org/10.31961/eltikom.v8i1.1105

Prasetiyo, E. E., Marausna, G., & Nugroho, D. W. (2022). 200 WP solar panel power plant optimization using dual-axis solar tracker system. *Jurnal Nasional Teknik Elektro dan Teknologi Informasi*, *11*(3), 215–221. https://doi.org/10.22146/jnteti.v11i3.4143

Prince, M. J., & Felder, R. M. (2006). Inductive teaching and learning methods: Definitions, comparisons, and research bases. *Journal of Engineering Education*, *95*(2), 123–138. https://doi.org/10.1002/j.2168-9830.2006.tb00884.x

Reda, I., & Andreas, A. (2004). Solar position algorithm for solar radiation applications. *Solar Energy*, *76*(5), 577–589. https://doi.org/10.1016/j.solener.2003.12.003

Rubio, F. R., Ortega, M. G., Gordillo, F., & López-Martínez, M. (2007). Application of new control strategy for sun tracking. *Energy Conversion and Management*, *48*(7), 2174–2184. https://doi.org/10.1016/j.enconman.2006.12.020

Saltelli, A., Aleksankina, K., Becker, W., Fennell, P., Ferretti, F., Holst, N., Li, S., & Wu, Q. (2019). Why so many published sensitivity analyses are false: A systematic review of sensitivity analysis practices. *Environmental Modelling & Software*, *114*, 29–39. https://doi.org/10.1016/j.envsoft.2019.01.012

Sandve, G. K., Nekrutenko, A., Taylor, J., & Hovig, E. (2013). Ten simple rules for reproducible computational research. *PLOS Computational Biology*, *9*(10), e1003285. https://doi.org/10.1371/journal.pcbi.1003285

Seme, S., Štumberger, B., Hadžiselimović, M., & Sredenšek, K. (2020). Solar photovoltaic tracking systems for electricity generation: A review. *Energies*, *13*(16), 4224. https://doi.org/10.3390/en13164224

Servant-Miklos, V. F. C., & Kolmos, A. (2022). Student conceptions of problem and project based learning in engineering education: A phenomenographic investigation. *Journal of Engineering Education*, *111*(4), 792–812. https://doi.org/10.1002/jee.20478

Shang, H., & Shen, W. (2023). Design and implementation of a dual-axis solar tracking system. *Energies*, *16*(17), 6330. https://doi.org/10.3390/en16176330

Skoplaki, E., & Palyvos, J. A. (2009). On the temperature dependence of photovoltaic module electrical performance: A review of efficiency/power correlations. *Solar Energy*, *83*(5), 614–624. https://doi.org/10.1016/j.solener.2008.10.008

Soedjangi, M. A. F. A.-A. (2025). Perancangan solar tracker dual-axis dengan monitoring intensitas cahaya, arus, tegangan, daya, dan sudut kemiringan panel surya berbasis IoT. *Infomatek*, *27*(1), 59–70. https://doi.org/10.23969/infomatek.v27i1.23992

Tan, M.-H., Wang, T.-K., Wong, C.-W., Chong, K.-K., Lim, B.-H., Yew, T.-K., Tan, W.-C., & Lai, A.-C. (2021). Comprehensive methodology to evaluate parasitic energy consumption for different types of dual-axis sun tracking systems. *International Journal of Photoenergy*, *2021*, 2870386. https://doi.org/10.1155/2021/2870386

Tembrevilla, G., Phillion, A., & Zeadin, M. (2024). Experiential learning in engineering education: A systematic literature review. *Journal of Engineering Education*, *113*(1), 195–218. https://doi.org/10.1002/jee.20575

Wendryanto, W., Widayana, G., & Sutaya, I. W. (2017). Pengembangan penggerak solar panel dua sumbu untuk meningkatkan daya pada solar panel tipe polikristal. *Jurnal Pendidikan Teknik Mesin Undiksha*, *5*(3). https://doi.org/10.23887/jjtm.v5i3.20293

Widjonarko, W., Laagu, M. A., & Fauzi, A. N. (2024). Desain dan implementasi sistem tracking dual-axis panel surya 50 Wp untuk optimalisasi daya. *Jurnal FORTECH*, *5*(2), 95–103. https://doi.org/10.56795/fortech.v5i2.5206

Yao, Y., Hu, Y., Gao, S., Yang, G., & Du, J. (2014). A multipurpose dual-axis solar tracker with two tracking strategies. *Renewable Energy*, *72*, 88–98. https://doi.org/10.1016/j.renene.2014.07.002